# Airfoil Shape and Thickness Effects on Transonic Airloads and Flutter

Samuel R. Bland* and John W. Edwards†
*NASA Langley Research Center, Hampton, Virginia*

**A transient pulse technique is used to obtain harmonic forces from a time-marching solution of the complete unsteady transonic small-perturbation potential equation. The unsteady pressures and forces acting on a model of the NACA 64A010 conventional airfoil and the MBB A-3 supercritical airfoil over a range of Mach numbers are examined in detail. Flutter calculations at constant angle of attack show a similar flutter behavior for both airfoils, except for a boundary shift in Mach number associated with a corresponding Mach number shift in the unsteady aerodynamic forces. Differences in the static aeroelastic twist behavior for the two airfoils are significant.**

## Nomenclature

$a$ = pitch axis location, referenced to midchord, in semichords
$b$ = semichord length
$c$ = chord length
$c_l$ = lift coefficient
$c_{l_h}$ = lift coefficient due to plunge
$c_{l_\alpha}$ = lift coefficient due to pitch
$c_m$ = moment coefficient about $c/4$
$c_{m_h}$ = moment coefficient due to plunge
$c_{m_\alpha}$ = moment coefficient due to pitch
$C_p$ = pressure coefficient
$g$ = structural damping coefficient
$h$ = plunge displacement in semichords
$h_l$ = plunge amplitude in semichord
$k$ = reduced frequency, $b\omega/V$
$M$ = freestream Mach number
$m$ = airfoil mass per unit span
$r_\alpha$ = radius of gyration, referenced to pitch axis, in semichords
$s$ = Laplace transform variable
$t$ = time
$V$ = freestream velocity
$x$ = streamwise coordinate
$x_s$ = shock location
$x_\alpha$ = center-of-gravity location, referenced to pitch axis, in semichords
$z$ = coordinate normal to stream
$\alpha_0$ = mean angle of attack, deg
$\alpha_l$ = amplitude of pitch oscillation, deg
$\Delta\alpha_e$ = static elastic twist angle, deg
$\Delta C_p$ = pressure coefficient, normalized by modal amplitude
$\mu$ = mass ratio, $m/\pi\rho b^2$
$\rho$ = air density
$\tau$ = nondimensional time, $Vt/b$
$\phi$ = phase angle, deg
$\omega$ = oscillation frequency
$\omega_h$ = uncoupled plunge mode frequency
$\omega_\alpha$ = uncoupled pitch mode frequency

Received March 10, 1983; revision received Oct. 19, 1983. This paper is declared a work of the U.S. Government and therefore is in the public domain.

*Aerospace Technologist, Unsteady Aerodynamics Branch. Associate Fellow AIAA.
†Head, Unsteady Aerodynamics Branch. Member AIAA.

## Introduction

THE calculation of aeroelastic response in the transonic regime continues to be an active area of research because of the significance of flutter in this speed range. Finite difference codes now allow the analyst to include the nonlinear aerodynamic effects associated with shock wave formation and motion. These codes have been most completely developed for the two-dimensional, small-perturbation potential flow equation. The LTRAN2 code[1] and its extensions have been widely used for this purpose. Edwards et al.[2] summarized applications of the finite difference codes to the flutter problem. In the present paper, a version of the LTRAN2 code, which incorporates higher frequency effects,[3] is used.

The aerodynamic forces generated by a time-marching, finite difference code can be incorporated into a flutter analysis in several ways. Classical solutions employ the forces for harmonic motion in each vibration mode in an eigenvalue analysis to determine the flutter point. The finite difference codes may be used to generate forces for such an application by forcing the airfoil to oscillate in the prescribed mode at the desired frequency and marching the solution in time until the transients have decayed and a periodic solution is achieved. This method requires that the code be run several times to obtain a single flutter point. A second approach is to couple the structural and aerodynamic equations and time-march the complete system from an initial disturbance. The stability is assessed from the growth or decay of the resulting transient response. Again, several runs of the code are required to determine the neutral stability point. A third approach is to compute the harmonic forces from the Fourier transform of the indicial response; that is, a step change in the mode is used as the initial condition, and the solution is time-marched until the transient has decayed.

A transient pulse technique,[3] which is a variation of the indicial response method, is used in this paper to obtain the aerodynamic forces. The Fourier transform of the resulting force response is divided by the transform of the airfoil motion to obtain the harmonic transfer function. A Padé fit of these $k$-plane forces is made to obtain an $s$-plane representation. A root locus solution is then used to determine the stability boundary. This procedure has the advantage that the expensive aerodynamic code need be run only once for each Mach number, mean angle of attack, and vibration mode. Subsequent flutter calculations for variations in structural parameters are relatively inexpensive. The applicability of the linear transform techniques to this nonlinear problem described above is verified by comparing the results with forced harmonic and transient aeroelastic solutions.

Edwards et al.[2] have shown a striking difference in the flutter behavior of a conventional and a supercritical airfoil in which the latter shows a curl back in the flutter speed vs Mach number when static aeroelastic twist is included. In this paper, the flutter behavior of a model of the NACA 64A010 conventional airfoil and the MBB-A3 supercritical airfoil is examined in detail for one mean angle of attack. The associated unsteady pressures and forces are presented. Similarities and differences between the aerodynamics of the two airfoils are interpreted to explain the flutter behavior.

## Aerodynamic Method

All calculations were made with the XTRAN2L[3] time-marching, finite difference code which solves the complete unsteady transonic small-perturbation potential equation. This code is an enhanced version of the LTRAN2-NLR[4] code that includes all of the appropriate time-dependent terms in the differential equation and boundary conditions. The alternating-direction implicit algorithm of Rizzetta and Chin[5] is used in a three-time-level scheme to treat the second-order time derivative in the differential equation. The low-frequency far-field radiation boundary conditions of Engquist and Majda[6] have been extended to the full-frequency equation and incorporated into XTRAN2L.

The XTRAN2L code uses a default $80\times61$ computational $x$-$z$ grid with 51 points on the airfoil. The points are uniformly spaced over the airfoil with the exception of an additional point near the leading edge. The grid extends 20 chord lengths upstream and downstream from the airfoil and 25 chord lengths above and below the airfoil. Reference 3 points out the necessity of stretching the grid smoothly away from the airfoil and of maintaining adequate grid resolution in the far field to avoid erroneous internal grid reflection of the outgoing waves. Details of the XTRAN2L code and the demonstration of its accuracy are given in Ref. 3.

## Results

Calculations were made for two airfoils at Mach numbers from 0.75 to 0.80 in increments of 0.01. The airfoils were the model of the NACA 64A010 tested at NASA Ames Research Center[7] (called 64AMES herein) and the supercritical MBB-A3 of German design. These airfoils are two of the AGARD standard configurations.[8] The 64AMES airfoil differs from the symmetric 10% thick NACA 64A010 airfoil in that the former is about 10.6% thick and has a small amount of camber. The MBB-A3 airfoil is an 8.9% thick, aft-loaded supercritical airfoil. The ordinates of both airfoils are given in Ref. 8. The airfoil slopes required by the aerodynamic code were obtained from cubic spline fits to the airfoil abscissas and ordinates, using an approximation to airfoil arc length as the independent variable. All calculations were made at mean angles of attack of $\alpha_0 = 1$ deg for the 64AMES airfoil and $\alpha_0 = -0.5$ deg for the MBB-A3 airfoil.

### Steady Aerodynamics

The steady-state pressure distributions for the two airfoils are shown in Fig. 1. The steady angle of attack for each airfoil was chosen such that the shock location and lift were about equal at the same Mach number. However, the shock strength is much less on the aft-loaded supercritical airfoil. Figure 2 gives the static aerodynamic parameters as functions of Mach number. As noted above, the lift coefficients and shock locations are approximately equal, although the lift increases more rapidly with Mach number on the 64AMES airfoil. As expected, the pitching moments (about the quarter chord) are quite different due to the aft loading on the supercritical MBB-A3 airfoil.

### Unsteady Aerodynamics

Pressure distributions and generalized aerodynamic forces were computed for harmonic oscillations in two modes, pitch about the quarter chord and vertical translation (plunge). All calculations were made for constant mean angle of attack. For harmonic oscillation of amplitude $\alpha_I$ the pitch motion is given by

$$\alpha(\tau) = \alpha_0 + \alpha_I \sin k\tau$$

where $k = b\omega/V$ is the reduced frequency based on semichord and $\tau = Vt/b$ is the nondimensional time. The plunge displacement is given by

$$h(\tau) = h_I \sin k\tau$$

where $h_I$ is nondimensional plunge amplitude.

Flutter calculations generally require the determination of generalized aerodynamic forces for a range of frequencies for each structural vibration mode. Harmonic airloads may be calculated with the XTRAN2L code by specifying the mode of motion and frequency of oscillation. Typically four cycles of oscillation are sufficient for the unwanted transients to die out. Fourier analysis of the last cycle of oscillation gives the Fourier harmonic components of the response. Each such calculation may require as many as 1440 time steps. Because the flutter analyst is interested in the forces for a range of frequencies, the use of an indicial method is attractive. Here the Fourier transform is used to provide the response at all frequencies of interest from a single transient response. A variation of this approach is used herein.

*Pulse Technique*

The indicial response is the response to a step function change in angle of attack. For the equation solved by the

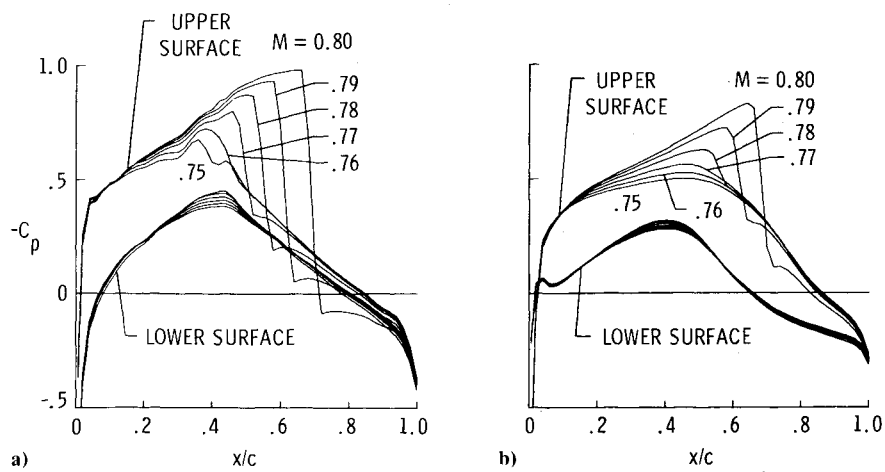


**Fig. 1 Steady pressure distributions; a) 64AMES airfoil, $\alpha_0 = 1$ deg, b) MBB-A3 airfoil, $\alpha_0 = -0.5$ deg.**

XTRAN2L code with the second-order time derivative included, the resulting response includes nonphysical transients due to the approximation of the infinite initial derivative using the finite time steps taken. For this reason a smoothly varying exponentially shaped pulse[3] is used. The input pulse in angle of attack is given by

$$\alpha(\tau) = \alpha_0 + \alpha_1 \exp[-(\tau - 17.5\Delta\tau)^2/4]$$

where $\Delta\tau$ is the nondimensional time step ($\alpha_1 = 0.5$ deg and $\Delta\tau = 5\pi/32$ were used).

An example of the input pulse and resulting lift and moment response for the 64AMES airfoil at $M = 0.8$ is shown in Fig. 3. The forces have not returned to their initial values for the 128 time steps shown. It is essential that the calculation be carried out to sufficient time for the transient to decay completely for the following reason. The harmonic response is obtained from the fast Fourier transforms (FFT) of the input and the response. If the final value of the time history has not returned to the initial value, the low-frequency results will be seriously in error. In practice 2048 steps were used, although 1024 steps were sometimes sufficient. The FFT technique provides forces up to the Nyquist frequency of $k = \pi/\Delta\tau = 6.4$. The accuracy of the method for frequencies as high as $k = 2$ is demonstrated in Ref. 3.

Steady results may be obtained from the XTRAN2L code using either the steady, successive line over-relaxation solver, or the unsteady solver with fixed airfoil geometry and time-marching to a steady state. These options lead to different steady-state results as indicated in Fig. 4 for the 64AMES airfoil at $M = 0.8$. Here the steady solver was run to convergence with a lift coefficient $c_l = 0.3461$ obtained. The unsteady solver was then used (with the airfoil held fixed), which resulted in the transient shown in Fig. 4. As was the case for the pulse described in the preceding paragraph, it was necessary to calculate several thousand time steps for this transient to decay. The transient shown was for the first 512 time steps. The resulting lift coefficient at convergence was $c_l = 0.3354$. It is, therefore, necessary to run the unsteady solver with fixed airfoil before applying the pulse technique described above in order to insure that the initial and final conditions for the pulse are the same.

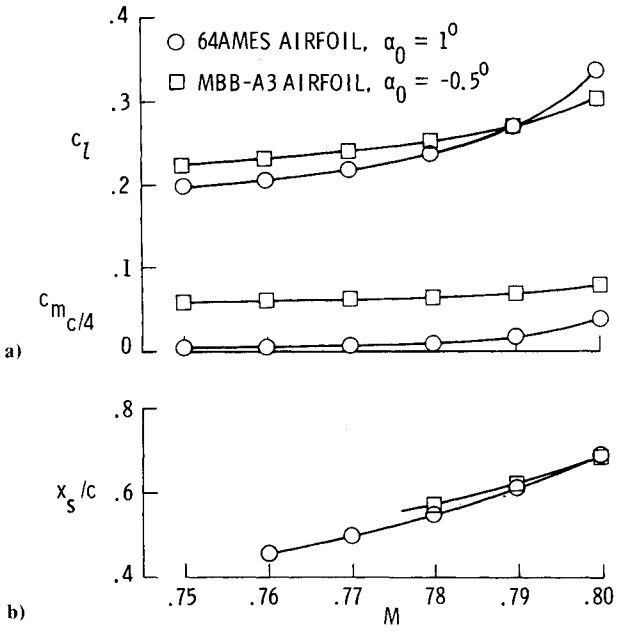


**Fig. 2 Steady aerodynamic parameters; a) force coefficients, b) shock location.**

*Harmonic Forces*

The harmonic forces were obtained using the pulse technique by performing an FFT of the pulse input (Fig. 3a) and of the force output (Fig. 3b) and dividing the latter by the former. For a case with 2048 time steps this leads to a frequency resolution of $\Delta k = 1/160$. A typical result is shown in Fig. 5. The real and imaginary components of the four force coefficients are presented for two cases—the 64AMES airfoil at $M = 0.78$ and the MBB-A3 airfoil at $M = 0.79$. The most striking result is the agreement in the forces for these two different airfoils at the different Mach numbers. This agreement in the forces with a 0.01 shift in $M$ holds true across the Mach number range for the cases treated in this paper. As may be anticipated, this comparison will be reflected in the flutter results to be shown later. The jagged nature of the curves at low frequency is not a serious problem in flutter analysis for which $k$ is usually greater than 0.1.

*Oscillation Amplitude Effects*

The lifting pressure distribution on the 64AMES airfoil at $M = 0.78$ oscillating in pitch at four different amplitudes is shown in Fig. 6. The first harmonic only is shown. These results were obtained from forced harmonic oscillation of the airfoil at $k = 0.15$. The pressure pulse seen near 55% chord is a result of the shock wave motion. The greatest nonharmonic response occurred at the aft end of the shock pulse and was as large as the fundamental component for $\alpha_1 = 2$ deg. Away from the shock, the response was nearly all at the fundamental frequency.

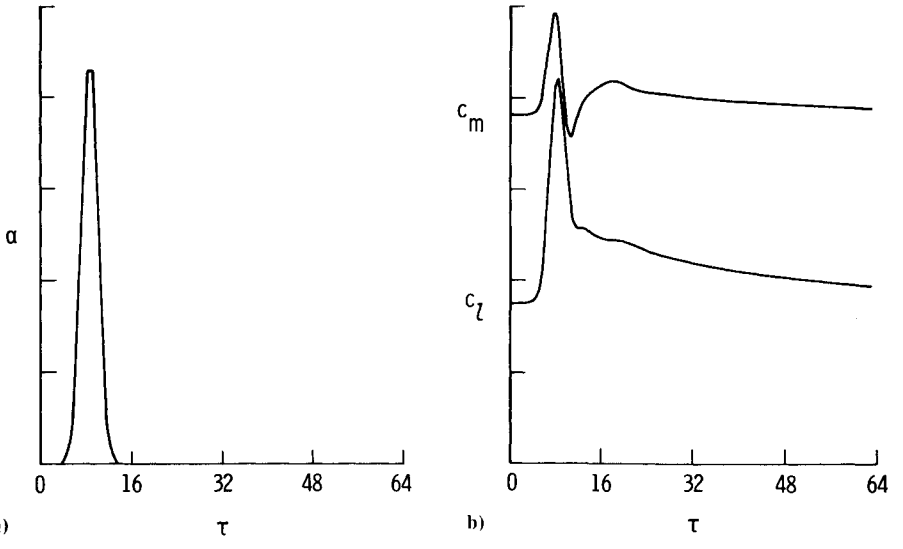


**Fig. 3 Transient pulse technique; a) angle-of-attack pulse, b) aerodynamic force response.**

A phase jump of about 120 deg occurs at the aft end of the shock pulse. Away from the shock, the phases and normalized magnitudes are essentially equal. The width of the pulse increases while the height decreases with increasing $\alpha_I$ in such a way that the overall forces remain nearly equal; that is, the force coefficients are independent of the amplitude of oscillation. The maximum differences in magnitude and phase for the cases shown are about 0.5% and 1 deg for lift and 6.4% and 7 deg for moment.

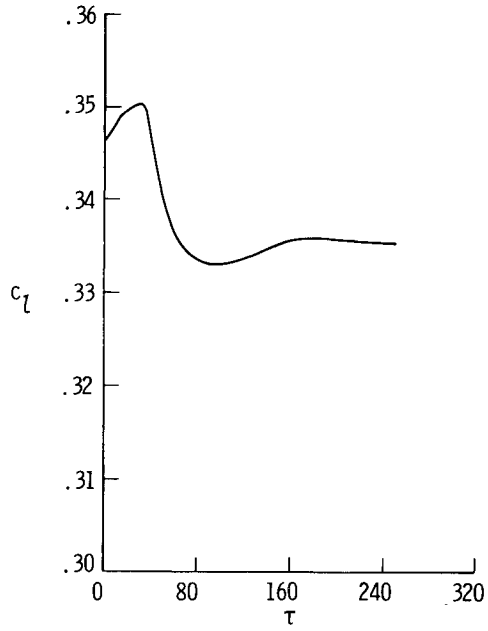


**Fig. 4 Transient force for unsteady solution with $\alpha_0 = 1$ deg held fixed; 64 AMES airfoil at $M = 0.8$.**

*Harmonic Airloads*

Calculations for forced harmonic motion were made for the plunge and pitch modes at each Mach number for both airfoils at $k = 0.15$. The plunge amplitude was $h_I = 0.02$ and the pitch amplitude was $\alpha_I = 0.5$ deg. The magnitude and phase of the lifting pressure coefficients (normalized by modal amplitude) for these cases are shown in Fig. 7 for the pitch mode and Fig. 8 for the plunge mode. The chief difference between the two airfoils is in the strength of the shock pulses; the location is about the same. This result might be anticipated from the corresponding steady pressures shown in Fig. 1. At the same Mach number, the phase jump at the shock is somewhat less for the MBB-A3 airfoil than for the 64AMES airfoil for the same reason.

The unsteady forces that result from these pressure distributions at $k = 0.15$ are shown in Figs. 9 and 10. Linear theory results from kernel function calculations for a flat plate airfoil are also shown. The lift coefficients (Fig. 9) for both airfoils show only mild changes with Mach number and agree quite well. The moment coefficients do show significant changes with Mach number. The most interesting observation from these two figures is the agreement between the two sets of calculations when the results for the MBB-A3 airfoil are shifted to a 0.01 lower Mach number. That is, the forces for the two airfoils are nearly equal across the Mach number range if the square symbols are shifted 0.01 Mach number to the left. This conclusion was anticipated in Fig. 5, which shows that this result holds over a wide frequency range.

In order to verify the accuracy of the pulse technique, the forces shown in Figs. 9 and 10 were compared with those obtained from pulses in $h$ and $\alpha$. The maximum differences in

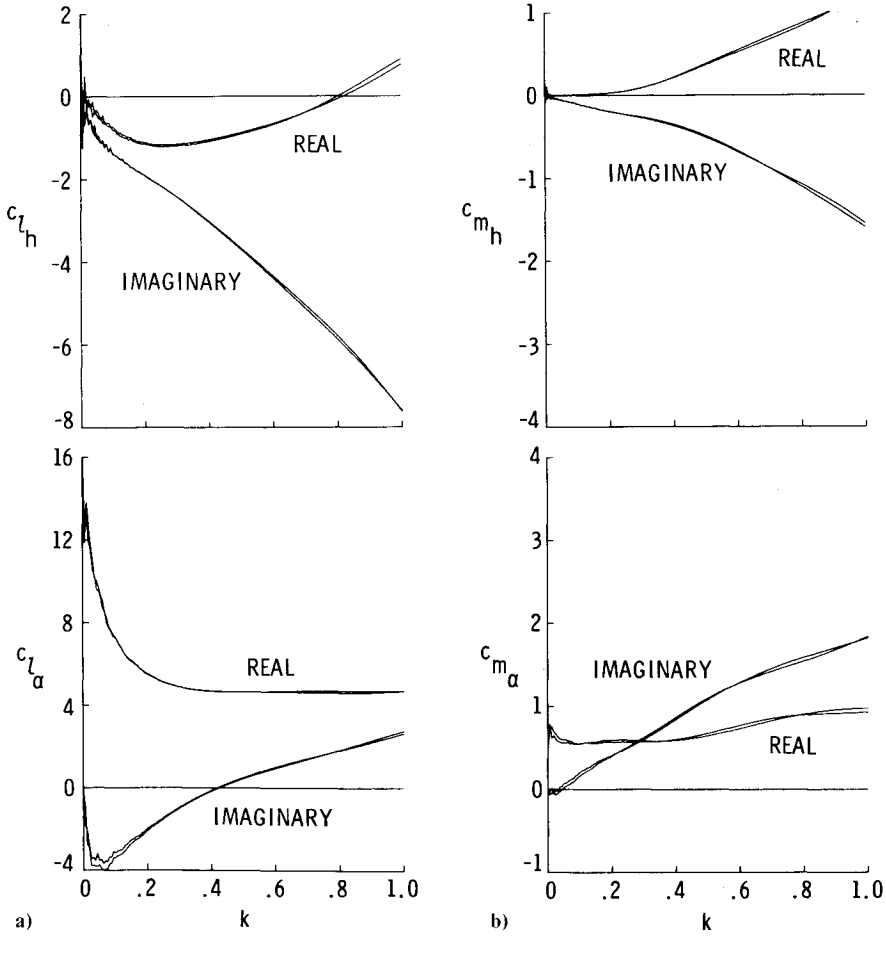


**Fig. 5 Comparisons of unsteady aerodynamic forces for 64AMES airfoil at $M = 0.78$ and MBB-A3 airfoil at $M = 0.79$; a) force coefficients, b) moment coefficients.**

magnitude occurred for the pitch case and were 0.048 for $c_{l_\alpha}$ and 0.018 for $c_{m_\alpha}$. The maximum phase difference was 3 deg.

**Flutter**

Flutter boundaries were calculated for each airfoil at each Mach number and one mean angle of attack ($\alpha_0 = 1$ deg for the 64AMES airfoil and $\alpha_0 = -0.5$ deg for the MBB-A3 airfoil). The structural parameters were those of Isogai's Case A[9] which were used in Ref. 2. The elastic-axis location was at $a = -2$, the center of gravity at $x_\alpha = 1.8$, and the radius of gyration squared was $r_\alpha^2 = 3.48$. The mass ratio was $\mu = 60$ and the modal frequencies were $\omega_h = \omega_\alpha = 100$ rad/s.

*Flutter Solution Method*

The XTRAN2L code may be used to obtain aeroelastic solutions by time-marching the coupled aerodynamic and structural equations.[2] This method requires several runs of the code to determine the neutral stability (flutter) point. Alternatively, the harmonic forces obtained from the pulse technique described herein may be used in a conventional *V-g* flutter analysis. The harmonic forces (*k* plane) may also be represented in the Laplace variable (*s* plane), and root locus methods may be used to determine the flutter behavior. In this paper, a Padé fit[10] was used to obtain the *s*-plane representation. It was necessary to use care in applying this method because of inaccuracies in the *k*-plane forces at very low frequencies ($k < 0.1$). There is also some question as to the suitability of the particular form of fit for transonic airloads.

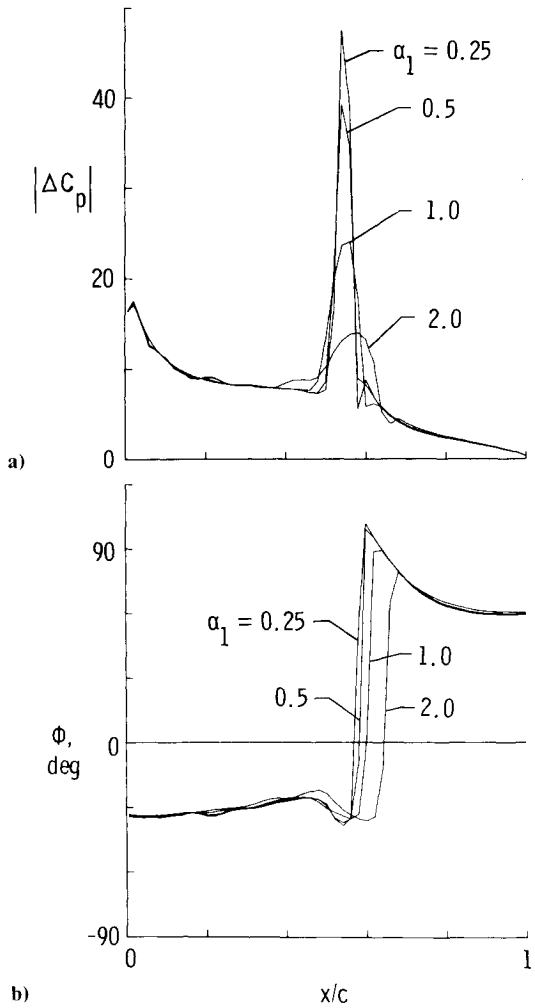


**Fig. 6 Pitch amplitude effect for 64AMES airfoil at $M = 0.78$, $k = 0.15$; a) magnitude, b) phase.**

In spite of these reservations, the method was used successfully by insuring that the Padé fit was accurate near the expected flutter frequency.

A sample root locus flutter solution for the 64AMES airfoil is shown in Fig. 11. The different curves were obtained by varying the speed. The symbols represent the time-marching aeroelastic solutions. The tick marks on the curves occur at speeds that correspond to those for the symbols. Excellent agreement is shown, which verifies the chain of linearity assumptions used in obtaining the curves; i.e., pulse transient to harmonic forces (via FFT) to root locus (via Padé fit).

*Flutter Results*

The flutter boundaries for the two airfoils are shown in Fig. 12 as flutter speed index $V/b\omega_\alpha\sqrt{\mu}$ and flutter reduced frequency as functions of Mach number. The Mach number range shown covers the region of the transonic dip, but does not extend past the point of minimum flutter speed. The potential flow calculations become unreliable beyond about $M = 0.8$ for the 64AMES airfoil. Difficulties with convergence of the aerodynamic code occur which appear to correlate with known problems of nonuniqueness with potential flow theory.[11,12] An example of this problem was observed in a calculation for the 64AMES airfoil at $M = 0.84$ and $\alpha_0 = 0$ deg for which a decidedly nonsymmetric pressure distribution was obtained; the upper and lower surface shocks were located at $x/c = 0.82$ and 0.69, respectively. For this airfoil at $M = 0.81$ and $\alpha_0 = 1$ deg (the angle of attack for the flutter calculations) the upper surface shock was located at $x/c = 0.82$ after 2048 time steps and the solution was not converged. It appears that the time constant for such cases is extremely large. The solution may appear to be stable for several hundred chord lengths of travel but ultimately will converge to a "nonphysical" solution.

The flutter boundaries for the two airfoils (Fig. 12) are remarkably similar. If the boundary for the MBB-A3 airfoil is shifted to the left by 0.01 Mach number, the curves are nearly coincident. This result is to be expected in light of the nature of the aerodynamic forces shown earlier (Figs. 5, 9, and 10). The similarity in the flutter boundaries was surprising because of the differences in flutter behavior for the two airfoils reported in Ref. 2. Additional calculations made to explain these differences are described in the following paragraphs.

Figure 13 shows the present flutter boundaries as lines with the results from Ref. 2 and some additional calculations shown as symbols. The flagged-symbol points, taken from Ref. 2, were calculated using the LTRAN2-NLR code[4] and differ from the present XTRAN2L code results in 1) equation level (the second time derivative term in the governing equation was omitted), 2) finite difference grid (discussed in Ref. 3), and 3) airfoil slope calculation procedure. In addition, the NACA 64A010 was used rather than the 64AMES airfoil used herein. In an attempt to sort out these different effects, several new calculations were made.

The unflagged circles shown in Fig. 13 were computed for the NACA 64A010 airfoil using the XTRAN2L code. The difference between these points and the solid curve for the 64AMES airfoil is a thickness effect and is consistent with a transonic similarity shift of about 0.007 in $M$ corresponding to a ratio in thickness of 1.06 between the airfoils. The difference between the flagged and unflagged circles (both for the 64A010 airfoil) is due to the three code differences enumerated above.

The unflagged square symbols for the MBB-A3 airfoil, shown in Fig. 13, were obtained from the XTRAN2L code with the second time derivative term set to zero. The rather large difference between these symbols and the dashed curve for the MBB-A3 airfoil is due solely to the difference in equation level (item 1 above). The flagged and unflagged squares were computed using the same equation level and differ only in items 2 and 3 above. This difference is not large, but the results from Ref. 2 (flagged) do show a steeper

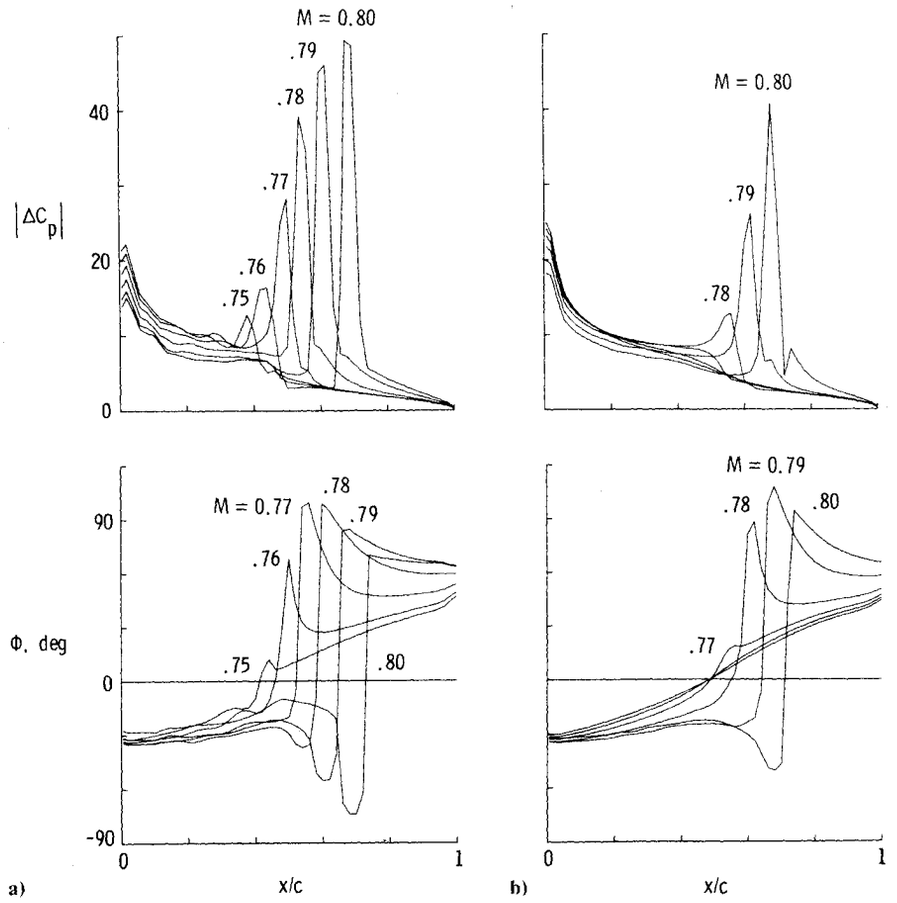


Fig. 7 Lifting pressure due to pitch about quarter chord at $k = 0.15$; a) 64AMES airfoil, b) MBB-A3 airfoil.

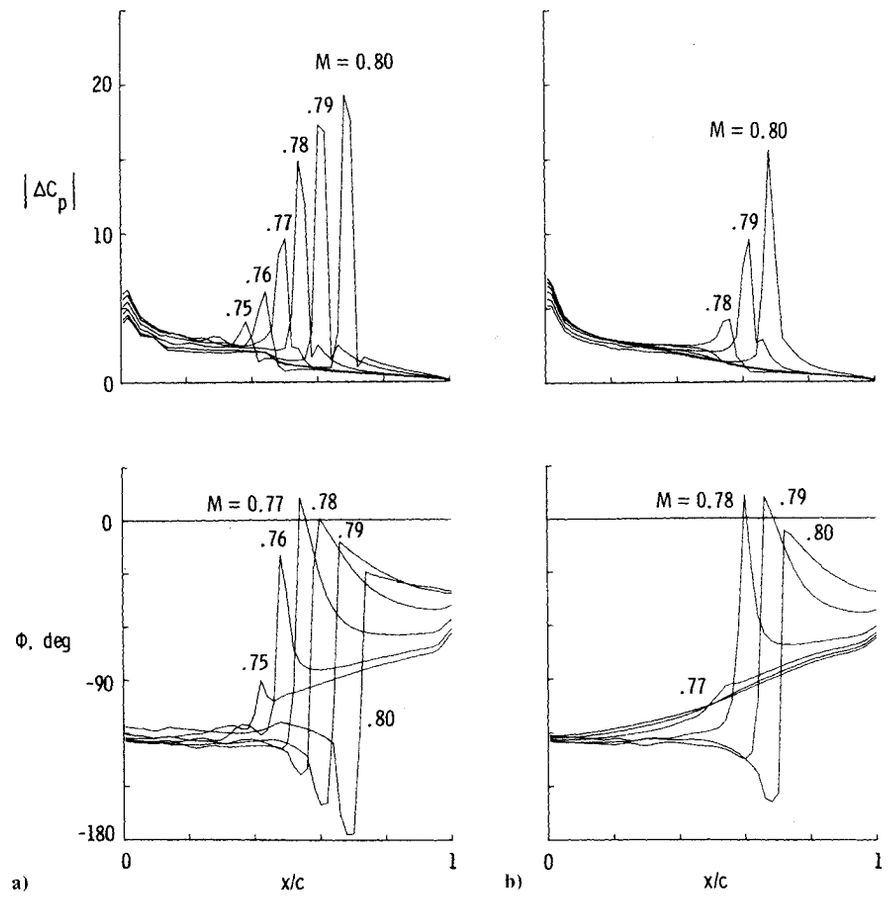


Fig. 8 Lifting pressure due to plunge at $k = 0.15$; a) 64AMES airfoil, b) MBB-A3 airfoil.

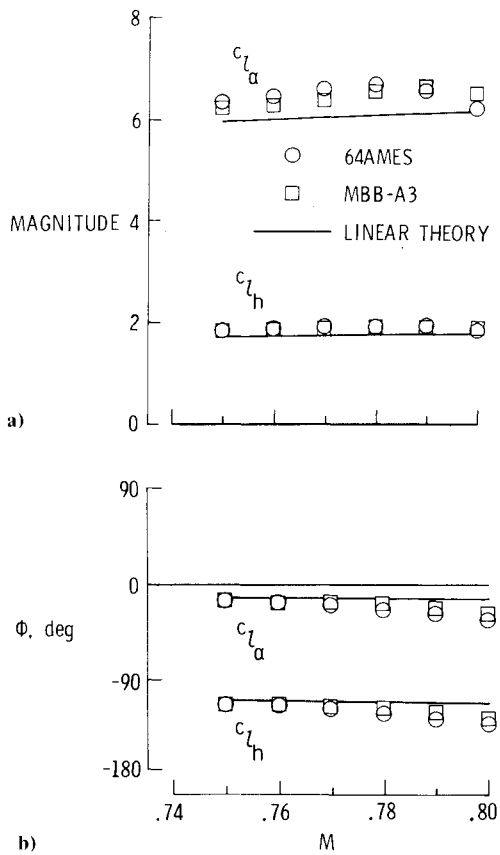


Fig. 9 Unsteady lift coefficient for $k = 0.15$.

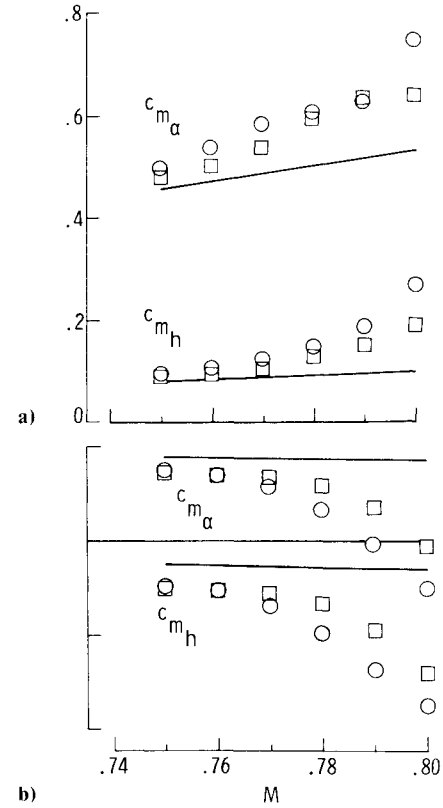


Fig. 10 Unsteady moment coefficient for $k = 0.15$.

transonic dip in flutter speed. In particular, at $M = 0.8$ the flutter speed from Ref. 2 (flagged square) has dropped below the speed computed from the same equation (unflagged square) herein. This difference in trend emphasizes the sensitivity of transonic calculations to the finite difference grid and airfoil slopes used.

*Static Aeroelastic Twist*

The flutter results shown in Figs. 12 and 13 were calculated holding the mean angle of attack of the section fixed. From a strip theory point of view, this would require a different root trim angle for each point because of the variations in flutter speed and in static pitching moment coefficient at each point. The elastic twist is computed from

$$\Delta\alpha_e = \alpha_0 - \alpha_r = \frac{2}{\pi r_\alpha^2}\left(\frac{V}{b\omega_\alpha\sqrt{\mu}}\right)^2 c_m(\alpha_0, M)$$

where $\alpha_0$ is the section angle of attack and $\alpha_r$ the unknown root angle required to balance the static aeroelastic moment. The pitching moment coefficient $c_m(\alpha_0, M)$ depends on $\alpha_0$ ($\alpha_0 = 1$ and $-0.5$ deg for the 64AMES and MBB-A3 airfoils, respectively) and on Mach number (as shown in Fig. 2 for $c_m$ referenced to $c/4$) and is referenced to the twist axis here.

Reference 2 showed a marked difference in behavior for the flutter of the conventional and supercritical airfoils with Mach number when the root trim angle was held fixed. (See Figs. 15 and 16 of Ref. 2 in which the $\alpha_0$ corresponds to $\alpha_r$ herein.) The determination of those results required calculation for several values of $\alpha_0$ and interpolation of the resulting root angles to obtain the desired $\alpha_r$. In this paper, all calculations were made for constant airfoil section angle $\alpha_0$. Using the root locus procedure, it was easy to vary the section

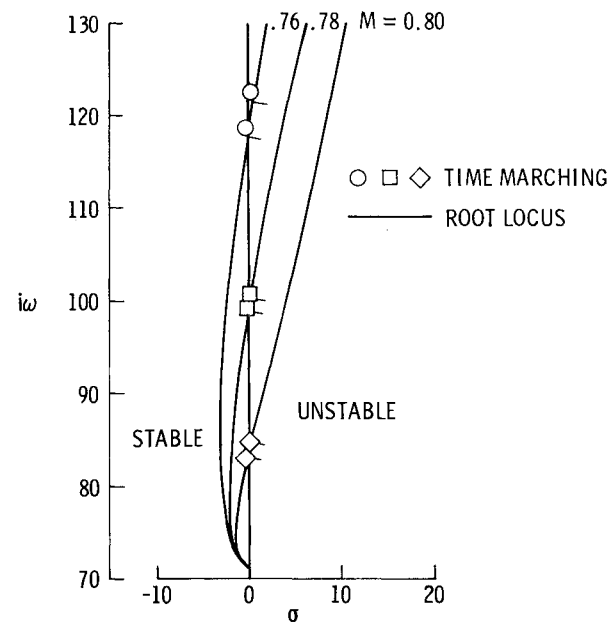


Fig. 11 Flutter root locus for 64AMES airfoil, $s = \sigma + i\omega$.

elastic axis location and the result of this variation on the static elastic twist is described below.

In Fig. 14 the elastic twist at flutter is shown for each airfoil for three elastic axis locations. The value $a = -2$ was used in all of the results shown earlier and the twist angles for these curves correspond to the flutter boundaries of Fig. 12. Comparing the two airfoils for $a = -2$, the MBB-A3 airfoil has a larger twist and shows a greater Mach number effect than does the 64AMES airfoil. The aeroelastic windup with $M$

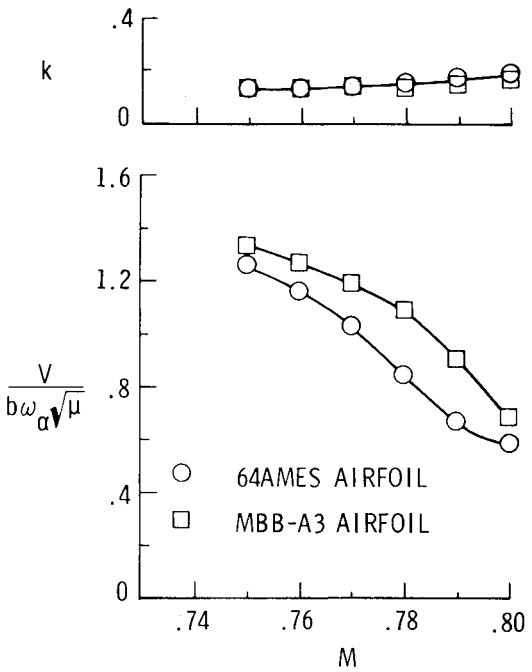


Fig. 12 Flutter results.

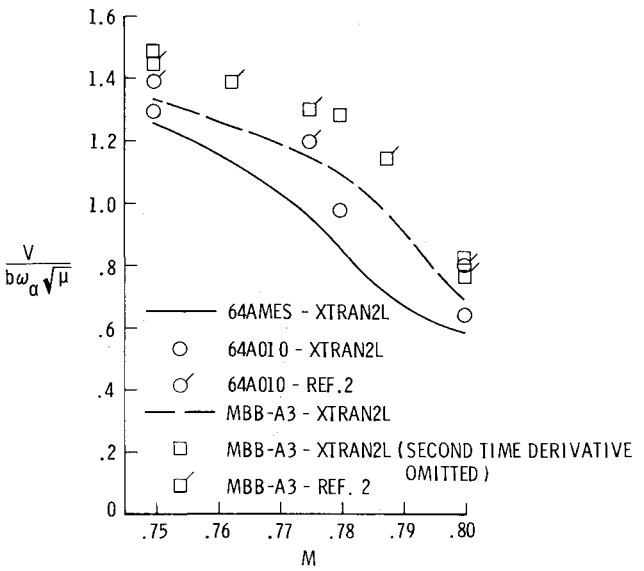


Fig. 13 Comparison of flutter boundaries.

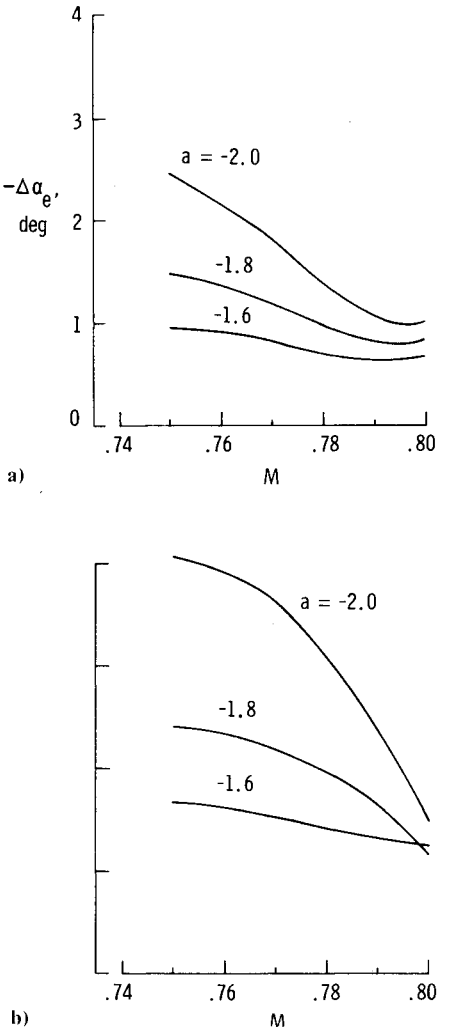


Fig. 14 Effect of elastic axis location on static aeroelastic twist; a) 64AMES airfoil, b) MBB-A3 airfoil.

of the MBB-A3 airfoil (2.5 deg) is about 1 deg greater than that of the 64AMES airfoil (1.5 deg). This greater twist is a result of the larger pitching moment coefficient for the supercritical airfoil (Fig. 2). If calculations were made for constant $\alpha_r$ one would expect the flutter similarities shown in Fig. 12 to disappear. The shapes of the flutter boundaries with Mach number would be quite different because the airfoil angle of attack $\alpha_0$ would change more for the MBB-A3 than for the 64AMES airfoil.

The value $a = -2$ places the pitch mode axis one semichord length ahead of the leading edge. As this axis is moved closer to the leading edge ($a = -1.8$ and $-1.6$), Fig. 14 shows the resulting decrease in elastic twist and a less severe Mach number trend. At $a = -1.6$, the two airfoils show nearly the same Mach number effect. For this variation the airfoil mass properties were held fixed, that is, $a + x_\alpha = -0.2$ in all cases.

## Conclusions

1) A transient pulse technique has been shown to be an accurate and efficient tool for determining aerodynamic forces for use in transonic flutter analysis. The necessity of carefully monitoring the convergence of the time-marching calculation is emphasized.

2) An *s*-plane Padé representation for the harmonic forces was used to provide a convenient and efficient means for performing parameter variations in flutter analysis. The technique used was sensitive to small inaccuracies in the harmonic forces at low frequencies.

3) Flutter boundaries were calculated for a conventional and a supercritical airfoil. The mean angles of attack were chosen such that the steady lift and shock locations were the same. The flutter boundaries were very similar except for a shift of about 0.01 in Mach number.

4) The unsteady forces for the two airfoils were compared at a reduced frequency ($k = 0.15$) in the flutter range. The lift coefficients were quite similar but the moment coefficients showed some differences. Again, a shift of 0.01 in Mach number brought the forces into reasonable agreement.

5) The unsteady pressure distributions for the two airfoils were also compared at a reduced frequency of 0.15. Although the shock strengths were different, the locations and widths of the shock pulses were very similar.

6) Unsteady pressure distributions for a range of pitch oscillation amplitudes showed that although the width of the

shock pulse increased with increased amplitude, the unsteady coefficients were nearly constant.

7) Calculations of the static aeroelastic twist at flutter were made for several pitch axis locations. The supercritical airfoil showed a greater variation of twist with Mach number than did the conventional airfoil.

## References

[1] Ballhaus, W.F. and Goorjian, P.M., "Implicit Finite-Difference Computations of Unsteady Transonic Flow About Airfoils," *AIAA Journal*, Vol. 15, Dec. 1977, pp. 1728-1735.

[2] Edwards, J.W., Bennett, R.M., Whitlow, W., Jr., and Seidel, D.A., "Time-Marching Transonic Flutter Solutions Including Angle-of-Attack Effects," *Proceedings, AIAA/ASME/ASCE/AHS 23rd Structures, Structural Dynamics and Materials Conference*, New Orleans, La., May 1982, pp. 220-233.

[3] Seidel, D.A., Bennett, R.M., and Whitlow, W., Jr., "An Exploratory Study of Finite-Difference Grids for Transonic Unsteady Aerodynamics," AIAA Paper 83-0503, Jan. 1983.

[4] Houwink, R. and van der Vooren, J., "Improved Version of LTRAN2 for Unsteady Transonic Flow Computations," *AIAA Journal*, Vol. 18, Aug. 1980, pp. 1008-1010.

[5] Rizzetta, D.P. and Chin, W.C., "Effect of Frequency in Unsteady Transonic Flow," *AIAA Journal*, Vol. 17, July 1979, pp. 779-781.

[6] Engquist, B. and Majda, A., "Numerical Radiation Boundary Conditions for Unsteady Transonic Flow," *Journal of Computational Physics*, Vol. 40, March 1981, pp. 91-103.

[7] Davis, S. S. and Malcolm, G. N., "Experimental Unsteady Aerodynamics of Conventional and Supercritical Airfoils," NASA TM 81221, Aug. 1980.

[8] Bland, S.R., "AGARD Two-Dimensional Aeroelastic Configurations," AGARD Advisory Rept. No. 156, Aug. 1979.

[9] Isogai, K., "Numerical Study of Transonic Flutter of a Two-Dimensional Airfoil," National Aerospace Lab., Japan, TR-617T, July 1980.

[10] Edwards, J. W., "Applications of Laplace Transform Methods to Airfoil Motion and Stability Calculations," *Proceedings, AIAA Structures, Structural Dynamics, and Materials Conference*, St. Louis, Mo., May 1979, pp. 465-481.

[11] Steinhoff, J. and Jameson, A., "Multiple Solutions of the Transonic Potential Flow Equation," *Proceedings, AIAA Computational Fluid Dynamics Conference*, Palo Alto, Calif., June 1981, pp. 347-353.

[12] Salas, M.D., Jameson, A., and Melnik, R.E., "A Comparative Study of the Nonuniqueness Problem of the Potential Equation," *Proceedings, AIAA Computational Fluid Dynamics Conference*, Danvers, Mass., July 1983, pp. 48-60.